The Astrophysical Journal, 865:38 (9pp), 2018 September 20 https://doi.org/10.3847/1538-4357/aad7fa

Halos in Dark Ages: Formation and Chemistry

B. Novosyadlyj[1,2,3], V. Shulga[1,3,4], W. Han[1,3], Yu. Kulinich[2], and M. Tsizh[2]
[1] International Center of Future Science of Jilin University, Qianjin Street 2699, Changchun, 130012, People's Republic of China
[2] Astronomical Observatory of Ivan Franko National University of Lviv, Kyryla i Methodia str., 8, Lviv, 79005, Ukraine
[3] College of Physics of Jilin University, Qianjin Street 2699, Changchun, 130012, People's Republic of China
[4] Institute of Radio Astronomy of NASU, 4 Mystetstv str., 61002 Kharkiv, Ukraine
Received 2018 July 12; revised 2018 August 1; accepted 2018 August 1; published 2018 September 18

Abstract

Formation of halos in the dark ages from initial spherical perturbations is analyzed in a four-component universe (dark matter, dark energy, baryonic matter, and radiation) in the approximation of relativistic hydrodynamics. Evolution of density and velocity perturbations of each component is obtained by integration of a system of nine differential equations from $z = 10^8$ up to virialization, which is described phenomenologically. It is shown that the number density of dark matter halos with masses $M \sim 10^8$–$10^9\,M_\odot$ virialized at $z \sim 10$ is close to the number density of galaxies in comoving coordinates. The dynamical dark energy of classical scalar field type does not significantly influence the evolution of the other components, but dark energy with a small value of effective sound speed can affect the final halo state. Simultaneously, the formation/dissociation of the first molecules has been analyzed in the halos that are forming. The results show that number densities of molecules H_2 and HD at the moment of halo virialization are $\sim 10^3$ and $\sim$400 times larger, respectively, than on a uniformly expanding background. This is caused by increased density and rates of reactions at quasi-linear and nonlinear evolution stages of density and velocity of the baryonic component of halos. It is shown also that the temperature history of the halo is important for calculating the concentration of molecular ions with low binding energy. Hence, in a halo with virial temperature $\sim 10^5$ K the number density of the molecular ion HeH^+ is approximately 100 times smaller than that on the cosmological background.

Key words: cosmology: theory – galaxies: formation – galaxies: high-redshift – hydrodynamics – intergalactic medium – stars: formation

1. Introduction

Molecules in the dark ages are an important subject of study for a few reasons. First of all, they are effective coolers of collapsing gas in the processes of the first stars' formation. Without a scrupulous account of their role in these processes, we cannot be sure that we know when the first sources of light appeared and which they were. Second, molecules are able to scatter and absorb the quanta of the cosmic microwave background and influence their energy and spatial distributions. They can be detected in the next-generation cosmic microwave background experiments. At last the dark ages molecules can be a source of light from the dark ages that brings new information about that epoch.

The growing list of molecules and possible reactions can be found in Dubrovich (1977), Izotov & Kolesnik (1984), Lepp & Shull (1984), Dalgarno & Lepp (1987), Puy et al. (1993), Galli & Palla (1998), Stancil et al. (1998), Puy & Signore (2002), Hirata & Padmanabhan (2006), Vonlanthen et al. (2009), Safranek-Shrader et al. (2010), and Gay et al. (2011). The current list of dark ages ingredients contains $\sim$30 species and $\sim$250 reactions (for reviews see Lepp & Stancil 1998; Lepp et al. 2002; Galli & Palla 2013). The main knowledge about primordial chemistry follows from the computations of cosmological recombination of hydrogen, deuterium, and helium and formation of neutral and ion molecules after recombination and before reionization by the first stars and galaxies ($10 \leqslant z \leqslant 1000$) in the ΛCDM model. It was shown that the number density of molecules in the dark ages crucially depends on the number density of free electrons and protons. The evaluation of ionized fractions depends on the accuracy of computation of all atomic and photonic processes during cosmological recombination, the existence of additional sources of ionization (e.g., decaying, annihilating dark matter particles), and the rate of expansion of the universe, which depends on the assumption about the nature of dark energy. It was shown also that only simple diatomic and triatomic molecules and molecular ions containing H, D, He, and Li are formed in trace amounts during the dark ages. Our recent computation for the ΛCDM model with Planck parameters (Planck Collaboration et al. 2016) in the case of an absence of sources of reionization before $z = 10$ showed that the relative number densities (in the units of hydrogen abundance) are 2.4×10^{-6} for molecule H_2, 1.1×10^{-9} for HD, 1.3×10^{-13} for H_2^+, and 8.5×10^{-14} for HeH^+ (Novosyadlyj et al. 2017). It was also found that the uncertainties of molecular abundances caused by the inaccuracies of computation of cosmological recombination are about 2%–3%. The uncertainties of values of cosmological parameters affect the abundances of molecules at the level of up to 2%.

The primordial molecules allow the gas to cool, contract, and fragment, which is very important for estimation of the mass function of the first luminous objects. Since the cosmological perturbations exist and evolve, the concentrations of the molecules change over time in different places in different ways. They are determined by the dynamics of change of baryonic density, temperature, radiation spectrum, and intensity and by the dependence of effective cross sections of molecular formation/destruction reactions on the physical state of the baryonic matter. The number densities of molecules decrease on a uniformly expanding background (further cosmological background or c.b.) and increase in the clouds that contract and virialize. We can compute the evolution of molecular number density on the c.b. with accuracy that is defined by accuracies of cosmological parameters (a few percent, as was mentioned above) and accuracies of cross sections, which are a bit less well known. At the same time, the computation of molecular fractions in the forming halos is less certain, since it is dependent on models of halo formation, which are mostly phenomenological in different aspects (see Lepp & Stancil 1998; Barkana & Loeb 2001; Lepp et al. 2002; Padmanabhan 2002; Bromm & Yoshida 2011; Galli & Palla 2013, and references therein).

In this paper, we study the formation of the first molecules in the halos that virialize at the end of the dark ages and compare molecular number densities with ones on the c.b. We describe the evolution of spherical perturbations in the multicomponent medium from the early stage when the corresponding peaks in the Gaussian field of cosmological perturbations as their seeds were superhorizon up to virialization of dark matter halos. Two models of baryonic gas behavior are considered: (i) when it is adiabatic at all stages, and (ii) when it reaches the virial temperature after virialization of the dark matter halo. In Section 2, we describe the model of spherical scalar perturbations in the four-component medium (dark matter, dark energy, baryonic gas, and thermal relic radiation), equations, initial conditions, the method of integration, and evolution of density and velocity perturbation amplitudes in the central part of spherical overdensities with baryonic mass $\sim 10^8$–$10^9\,M_\odot$. In Section 3, we analyze the formation of molecules in the halo and on the c.b. during the dark ages before reionization by first stars and compare them. Discussions and conclusions are presented in Section 4.

2. Formation of Halos in the Dark Ages

Let us analyze the evolution of spherical perturbations of galaxy scales in the four-ingredient universe (cold dark matter, baryonic matter, dark energy, and thermal relic radiation) from a linear stage in the early epoch, through the quasi-linear stage, the turnaround point, infall, and formation of spherical halos at the end of the dark ages. We use the hydrodynamical approximation in which each ingredient is a continuous medium with energy density $\varepsilon_{(N)}(t, r)$, pressure $p_{(N)}(t, r)$, equation-of-state parameter $w_{(N)} \equiv p_{(N)}(t, r)/\varepsilon_{(N)}(t, r)$, and squared effective sound speed $c^2_{s\,(N)} \equiv \delta p_{(N)}/\delta\varepsilon_{(N)}$. The cold dark matter, as usual, has dust-like parameters: $w_{\rm dm} = c^2_{\rm s\,(dm)} = 0$. For the dark energy, we assume $w_{\rm de} = {\rm const} = -0.9$ and $c^2_{\rm s(de)} = 1$ or $\ll 1$ (in units of the speed of light). The baryon–photon plasma at the radiation-dominated epoch is ultrarelativistic with $w_{\rm r,b} = c^2_{\rm s\,(r,b)} = 1/3(1 + R)$, where $R \equiv 3\varepsilon_{\rm b}/4\varepsilon_{\rm r}$ (Hu & Sugiyama 1995, 1996). After cosmological recombination the baryonic ingredient is practically neutral ideal gas with $w_{\rm b} = c^2_{\rm s(b)} = \tilde{\gamma} kT_{\rm b}/\mu_{\rm H} m_{\rm H}$, where $T_{\rm b}$ is its temperature, $m_{\rm H}$ is hydrogen atom mass, $\mu_{\rm H}$ is mass per H atom, k is Boltzmann's constant, and $\tilde{\gamma}$ is the adiabatic index, which we suppose here is equal to 5/3. We assume the standard primordial chemistry following from the cosmological nucleosynthesis with helium nucleon fraction $Y_p = 0.2465 \pm 0.0097$ (Aver et al. 2013). In the expanding homogeneous universe the density of ingredients follows the energy–momentum conservation law

$$\bar{\varepsilon}_{\rm dm}(t) = \varepsilon^{(0)}_{\rm dm} a^{-3}, \quad \bar{\varepsilon}_{\rm b}(t) = \varepsilon^{(0)}_{\rm b} a^{-3},$$
$$\bar{\varepsilon}_{\rm de}(t) = \varepsilon^{(0)}_{\rm de} a^{-3(1+w_{\rm de})}, \quad \bar{\varepsilon}_{\rm r}(t) = \varepsilon^{(0)}_{\rm r} a^{-4}, \tag{1}$$

where $a(t)$ is the scale factor normalized to 1 at the current moment of time t_0 ($a(t_0) = 1$) and $\varepsilon^{(0)}_{(N)}$ are the energy densities at the current epoch, which are usually parameterized by the dimensionless density parameters $\Omega_{(N)} = \bar{\varepsilon}^{(0)}_{(N)}/\varepsilon^{(0)}_{\rm (cr)}$, where the critical density $\varepsilon^{(0)}_{\rm (cr)} \equiv 3c^2H_0^2/8\pi G$. We will also use notation $\Omega_{\rm m} \equiv \Omega_{\rm dm} + \Omega_{\rm b}$. In the computations we assume the Hubble constant $H_0 = 70\ {\rm km\,s^{-1}\,Mpc^{-1}}$ and zero space curvature.

2.1. Equations of Evolution for Amplitudes of Spherical Perturbation and Initial Conditions

We suppose that the halo forms from spherical adiabatic perturbation, in which the density of each ingredient is $\varepsilon_{(N)}(t, r) = \bar{\varepsilon}_{(N)}(t)(1 + \delta_{(N)}(t, r))$ and the Friedmann–Lemaitre–Robertson–Walker metric is slightly perturbed,

$$ds^2 = e^{\nu(t,r)}dt^2 - a^2(t)e^{\nu(t,r)}[dr^2 + r^2 d\Omega^2], \tag{2}$$

where $d\Omega^2 = d\theta^2 + \sin^2\theta d\varphi^2$. In the early epoch $\delta_{(N)} \ll 1$ and $\nu \ll 1$. The components of four-velocity $u^{\rm i}_{(N)}(t, r) \equiv dx^{\rm i}_{(N)}/ds$ are connected with components of three-velocity $v^{\rm i}_{(N)}(t, r) \equiv dr_{(N)}/d\tau$, where $d\tau \equiv e^{\nu(t,r)}dt$ is an interval of proper time of the observer in the point of spacetime (t, r), by relations

$$u^{\rm i}_{(N)}(t, r) = \left\{\frac{e^{-\nu/2}}{\sqrt{1 - v^2_{(N)}}},\ \frac{e^{-\nu/2}v_{(N)}}{a\sqrt{1 - v^2_{(N)}}},\ 0,\ 0\right\}.$$

The components of the energy–momentum tensor of ideal fluid in the v^2-approximation are as follows:

$$T^0_{0\,(N)} = \varepsilon_{(N)} + (\varepsilon_{(N)} + p_{(N)})v^2_{(N)},$$
$$T^1_{0\,(N)} = a^{-1}(\varepsilon_{(N)} + p_{(N)})v_{(N)},$$
$$T^1_{1\,(N)} = -p_{(N)} - (\varepsilon_{(N)} + p_{(N)})v^2_{(N)},$$
$$T^2_{2\,(N)} = T^3_{3\,(N)} = -p_{(N)}.$$

The evolution of the c.b. and spherical perturbation is described by Einstein equations of general relativity and equations of energy–momentum conservation

$$R^{\rm i}_{\rm j} - \frac{1}{2}\delta^{\rm i}_{\rm j}R = \frac{8\pi G}{c^4}\sum_N T^{{\rm i}\,(N)}_{\rm j}, \quad T^{{\rm k}\,(N)}_{\rm i;k} = 0. \tag{3}$$

For the c.b. ($\nu = \delta_{(N)} = v_{\rm (N)} = 0$) they give the Friedmann equations

$$H = H_0\sqrt{\Omega_{\rm r}a^{-4} + \Omega_{\rm m}a^{-3} + \Omega_{\rm de}a^{-3(1+w_{\rm de})}}, \tag{4}$$
$$q = \frac{\Omega_{\rm r}a^{-4} + \Omega_{\rm m}a^{-3}/2 + (1 + 3w_{\rm de})\Omega_{\rm de}a^{-3(1+w_{\rm de})}}{\Omega_{\rm r}a^{-4} + \Omega_{\rm m}a^{-3} + \Omega_{\rm de}a^{-3(1+w_{\rm de})}},$$

which describe the dynamic of expansion of the universe in terms of its rate $H \equiv d\ln a/dt$ and deceleration parameters $q \equiv -d^2a/dt^2/H^2$. The integration of the first one from them gives the dependence $a(t)$ or/and $t(a)$. It is comfortable to use a as the independent variable instead t, since it is simply connected with redshift $z = 1/a - 1$, which is a measurable value. The derivative with respect to t is presented over the derivative with respect to a as follows: $d/dt = aHd/da$. For compactness below, we will use the notation $(\dot{}) \equiv \frac{d}{da}$.

The perturbed part of Equations (3) consists of the system of nine equations for nine unknown functions of a and r: $\nu(a, r)$, $\delta_{\rm dm}(a, r)$, $v_{\rm dm}(a, r)$, $\delta_{\rm b}(a, r)$, $v_{\rm b}(a, r)$, $\delta_{\rm de}(a, r)$, $v_{\rm de}(a, r)$, $\delta_{\rm r}(a, r)$, $v_{\rm r}(a, r)$. In this paper we are mainly interested in the densest central part of a halo formed in the dark ages. At the early epoch, the perturbations are small and equations of their evolution can be linearized for all ingredients. Moreover, each function of a and r can be presented as a product of its amplitude, which depends on a only, and some function of radial coordinate r, which describes the initial profile of spherical perturbation. The last can be expanded into a series of some orthogonal functions, e.g., spherical ones in our case. In particular, we can present the perturbations of the metric, density, and velocity of the N-ingredient as follows:

$$\nu(a, r) = \tilde{\nu}(a)\frac{\sin kr}{kr}, \quad \delta_{(N)}(a, r) = \tilde{\delta}_{(N)}(a)\frac{\sin kr}{kr},$$
$$v_{(N)}(a, r) = \tilde{v}_{(N)}(a)k\left(\frac{\cos kr}{kr} - \frac{\sin kr}{k^2r^2}\right). \tag{5}$$

For analyzing the evolution of the central part of the spherical halo, we can decompose the r-function in the Taylor series and keep only leading terms:

$$f_k(r) \approx 1, \quad f_k'(r) \approx -\frac{1}{3}k^2r, \quad f_k''(r) + \frac{2f_k(r)}{r} \approx -k^2,$$

where $f_k(r) = \sin kr/kr$. This gives the possibility of reducing the system of nine partial differential equation for unknown functions (5) to the system of nine ordinary differential equations for their amplitudes $\tilde{\nu}(a)$, $\tilde{\delta}_{\rm dm}(a)$, $\tilde{v}_{\rm dm}(a)$, $\tilde{\delta}_{\rm b}(a)$, $\tilde{v}_{\rm b}(a)$, $\tilde{\delta}_{\rm de}(a)$, $\tilde{v}_{\rm de}(a)$, $\tilde{\delta}_{\rm r}(a)$, $\tilde{v}_{\rm r}(a)$:

$$\dot{\tilde{\nu}} + \left(1 + (1 - \tilde{\nu})\frac{k^2}{3a^2H^2}\right)\frac{\tilde{\nu}}{a}$$
$$= -\frac{\Omega_{\rm m}\tilde{\delta}_{\rm m} + \Omega_{\rm r}a^{-1}\tilde{\delta}_{\rm r} + \Omega_{\rm de}a^{-3w_{(N)}}\tilde{\delta}_{\rm de}}{\Omega_{\rm m}a + \Omega_{\rm r} + \Omega_{\rm de}a^{1-3w_{(N)}}}, \tag{6}$$

$$\dot{\tilde{\delta}}_{(N)} + \frac{3}{a}(c_{s(N)}^2 - w_{(N)})\tilde{\delta}_{(N)}$$
$$- (1 + w_{(N)})\left[\frac{k^2\tilde{v}_{(N)}}{a^2H} + 9H(c_{s(N)}^2 - w_{(N)})\tilde{v}_{(N)} + \frac{3}{2}\dot{\tilde{\nu}}\right]$$
$$- (1 + c_{s(N)}^2)\left[\frac{k^2\tilde{\delta}_{(N)}\tilde{v}_{(N)}}{a^2H} + \frac{3}{2}\tilde{\delta}_{(N)}\dot{\tilde{\nu}}\right] = 0, \tag{7}$$

$$\dot{\tilde{v}}_{(N)} + (1 - 3c_{s(N)}^2)\frac{\tilde{v}_{(N)}}{a} + \frac{c_{s(N)}^2\tilde{\delta}_{(N)}}{a^2H(1 + w_{(N)})} + \frac{\tilde{\nu}}{2a^2H}$$
$$- \frac{4k^2\tilde{v}_{(N)}^2}{3a^2H} + \frac{1 + c_{s(N)}^2}{1 + w_{(N)}}[\dot{\tilde{\delta}}_{(N)}\tilde{v}_{(N)} + \tilde{\delta}_{(N)}\dot{\tilde{v}}_{(N)}$$
$$+ (1 - 3w_{(N)})\frac{\tilde{\delta}_{(N)}}{a}\tilde{v}_{(N)} + \frac{\tilde{\nu}\tilde{\delta}_{(N)}}{2a^2H}\bigg] = 0. \tag{8}$$

To take into account the Silk damping and drag effects for the baryon–photon plasma before and during recombination, we supplement the right-hand sides of Equations (7) and (8) for photons by terms $-k^2\tilde{\delta}_{\rm r}/a^2Hk_{\rm D}^2$ and $-k^2\tilde{v}_{\rm r}/a^2Hk_{\rm D}^2$ and for baryons by $-k^2\tilde{\delta}_{\rm b}/a^2Hk_{\rm D}^2e^{k^2/k_{\rm D}^2}$ and $-k^2\tilde{v}_{\rm b}/a^2Hk_{\rm D}^2e^{k^2/k_{\rm D}^2}$ correspondingly. The damping scale $k_{\rm D}$ we compute semianalytically according to Hu & Sugiyama (1995).

To integrate them, we should set the initial conditions for each function at a radiation-dominated epoch at $a_{\rm init} = 10^{-8}$ when cluster- and galaxy-scale perturbations are superhorizon. Linearized Equations (6)–(8) for the radiation component have asymptotic values at $a_{\rm init}$,

$$\tilde{\nu}^{\rm init} = -C_k, \quad \tilde{\delta}_{\rm r}^{\rm init} = C_k, \quad \tilde{v}_{\rm r}^{\rm init} = \frac{C_k}{4a_{\rm init}H(a_{\rm init})}, \tag{9}$$

where C_k is some constant. The solutions of Equations (6)–(8) for matter and dark energy as the test components give the asymptotic values for superhorizon perturbations at $a_{\rm init}$,

$$\tilde{\delta}_{\rm dm}^{\rm init} = \tilde{\delta}_{\rm b}^{\rm init} = \frac{3}{4}C_k, \quad \tilde{\delta}_{\rm de}^{\rm init} = \frac{3}{4}(1 + w_{\rm de})C_k,$$
$$\tilde{v}_{\rm m}^{\rm init} = \tilde{v}_{\rm b}^{\rm init} = \tilde{v}_{\rm de}^{\rm init} = \frac{C_k}{4a_{\rm init}H(a_{\rm init})}. \tag{10}$$

We will see that $k \sim 1$–$10\,{\rm Mpc}^{-1}$ scale perturbations can form the halo at $z \sim 30$–10 if their amplitudes $C_k \sim (1 - 3) \times 10^{-4}$. Let us compare these values with the rms amplitude that follows from the initial power spectrum normalized to Planck2015 data (Planck Collaboration et al. 2016).

The power spectrum of curvature perturbations is usually presented as $\mathcal{P}_R(k) = A_{\rm s}(k/0.05)^{n_{\rm s}-1}$ (Lewis et al. 2000), where $n_{\rm s}$ is the spectral index of the scalar mode of cosmological density perturbations and $A_{\rm s}$ is its amplitude at $k = 0.05\,{\rm Mpc}^{-1}$. Using the Planck2015 + *HST* + WiggleZ + SNLS3 data set, we have determined their mean values and 2σ confidence limits: $A_{\rm s} = 2.19^{+0.12}_{-0.10} \times 10^{-9}$, $n_{\rm s} = 0.960 \pm 0.013$ (Sergijenko & Novosyadlyj 2015). For the perturbations of superhorizon scales $\mathcal{P}_R \equiv \frac{9}{16}\langle\tilde{\nu}\cdot\tilde{\nu}\rangle = {\rm const}$ the rms value of metric perturbation $\sigma_\nu \equiv \langle\tilde{\nu}\cdot\tilde{\nu}\rangle^{1/2} \approx 5.7 \times 10^{-5}(k/5)^{\frac{n_{\rm s}-1}{2}}$. This means that the height of peaks in the Gaussian random field of matter density perturbations is $2\sigma_\nu$–$5\sigma_\nu$.

The system of Equations (6)–(8) should be supplemented by equations of evolution of temperature of the gas, since it determines the pressure and effective sound speed. At $z > 850$ the temperature of baryonic matter $T_{\rm b}$ practically equals the temperature of radiation $T_{\rm r}$, which adiabatically cools with expansion of the universe:

$$\frac{dT_{\rm b}}{dz} = \frac{T_{\rm b}}{1 + z}. \tag{11}$$

Hence, at $a_{\rm init} \leqslant a \leqslant 0.0012$ ($850 < z \leqslant z_{\rm init}$), $T_{\rm b} \approx T_{\rm r} = T_0a^{-1}$, where $T_0 = 2.7255 \pm 0.0006$ K (Fixsen 2009). At the lower redshifts, when $z \lesssim 850$, the baryonic matter is slightly connected with thermal background radiation via its Compton scattering on the residual fraction of free electrons. Since the cooling rate function of baryonic gas with primordial chemistry is negligible (see Figure 1 in Safranek-Shrader et al. 2010), the adiabatic cooling/heating of monomolecular gas, at last, becomes the main thermal process for it. At this stage the temperature of the baryonic matter can be described by the following equation:

$$\frac{dT_{\rm b}}{dz} = \frac{2T_{\rm b}}{1 + z}\left(1 + \frac{2}{3}\frac{d\tilde{\delta}_{\rm b}}{dz}\right)$$
$$+ \frac{8\sigma_{\rm T}a_{\rm r}T_{\rm r}^4}{3m_{\rm e}cH(1 + z)}\frac{x_{\rm e}}{1 + f_{\rm D} + f_{\rm He} + x_{\rm e}}(T_{\rm b} - T_{\rm r}), \tag{12}$$

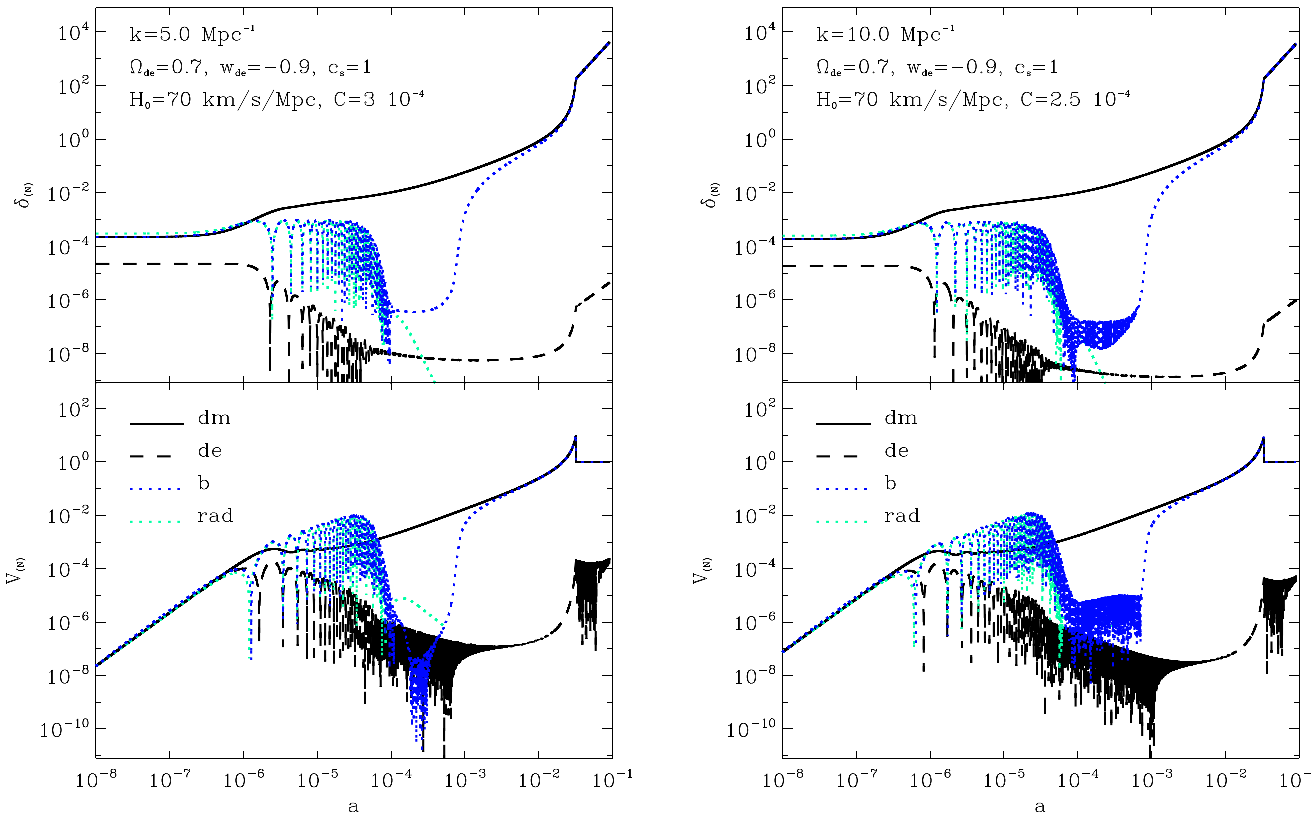

Figure 1. Evolution of density and velocity perturbations of the matter, dark energy, baryons, and radiation. Cosmological parameters here and below are as follows: $H_0 = 70$ km s^{-1} Mpc^{-1}, $\Omega_{de} = 0.7$, $w_0 = -0.9$, $c^2_{s(de)} = 1$, $\Omega_b = 0.05$, $\Omega_K = 0$, $T_0 = 2.7255$ K.

where x_e, f_{He}, and f_H are free electron, total helium, and total deuterium fractions, respectively (see Section 3 for details). The constants are the speed of light c, Thomson scattering cross section σ_T, electron mass m_e, and radiation constant a_r.

The system of Equations (6)–(8), (11), and (12) describes the evolution of density and velocity perturbations of each ingredient with initial conditions (9) and (10) at linear and nonlinear stages, turnaround, and infall, but without the final stage of halo formation—virialization.

2.2. Formation of Halos

Here we will not detail the final processes of the halo formation such as molecular cooling, fragmentation, star formation, and reionization (see, e.g., Oh & Haiman 2002; Safranek-Shrader et al. 2010; Demianski & Doroshkevich 2014), but we will use an approximate description of achievement of a state of dynamic equilibrium based on the virial theorem. It was shown that in the flat model with $\Omega_{de} \sim 0.7$ the overdensity of halos of dark matter $\Delta_v \equiv \varepsilon_{dm}(a_v, r = 0)/\bar{\varepsilon}_{dm}(a_v) - 1 \approx 177$ at the moment of virialization $a_v < 0.5$ (Kulinich & Novosyadlyj 2003). Hence, when $\tilde{\delta}_{dm}$ reach Δ_v we assume $\tilde{\delta}_{dm}(a \geqslant a_v, r = 0) = (\Delta_v + 1)(a/a_v)^3 - 1$ and $\tilde{v}_{dm}(a \geqslant a_v) = -\tilde{V}_H$, where $\tilde{V}_H = aH$ is the amplitude of Hubble velocity $V_H = aHr$ at the infinitesimal distance r from the center halo (for details, see Novosyadlyj et al. 2016). The baryonic matter during halo formation is first heated adiabatically and later by shock waves, if they are generated.

In Figure 1 we show the results of integration of Equations (6)–(8), (11), and (12) with initial conditions (9) and (10). The dynamical dark energy there is a classical scalar field. The evolution of amplitudes of density perturbation $\tilde{\delta}_{(N)}$ and velocity $\tilde{v}_{(N)}$ of each ingredient up to formation of a dark matter halo is presented there. In the left panel the scale of initial perturbation is $\lambda/2 = \pi k^{-1} \approx 0.6$ Mpc, in the right one $\approx$0.3 Mpc. They form the halos with mass of baryonic matter $\sim 10^9$ and $\sim 10^8\, M_\odot$, respectively, at redshift $\sim$30. The initial amplitudes of metric perturbations for them are -3×10^{-4} and -2.5×10^{-4}, which exceed the rms value by $\approx$5.3 and $\approx$4.4 times, respectively. Such peaks in the Gaussian random field of curvature perturbations are very rare. If the amplitudes are $\sim$2–3 times lower, then the perturbations of such scales form the halos at redshift $\sim$15–10. The number density of such halos is comparable to the mean number density of galaxies.

The evolution of mass matter density $\rho_m(a) = \rho_m^0(1 + \tilde{\delta}_m(a))a^{-3}$ and temperature of baryonic ingredient T_b in the central part of the halo are shown in Figure 2 (left column). The temperature of gas in the virialized halo is shown for two important cases: when it is heated by adiabatic compression only $T_b^{(ad)}$ (dark thick solid lines), and when it is heated by shocks in the processes of violent relaxation to virial temperature $T_b^{(vir)}$ (red thick solid lines). In the first case, the final temperature is a result of integration of Equation (12); in the second one, we set it by hand at $a \geqslant a_v$ from Barkana & Loeb (2001) and Bromm & Yoshida (2011):

$$T_b^{(vir)} = 2 \times 10^4 \left(\frac{\mu_H}{1.2}\right)\left(\frac{M_{halo}}{10^8\, M_\odot}\right)^{2/3}\left(\frac{\Delta_v}{178}\right)^{1/3}\left(\frac{0.1}{a_v}\right) \text{K}. \quad (13)$$

We suppose that the temperature of the gas in the real halos of different masses is in the range $T_b^{(ad)} \leqslant T_b \leqslant T_b^{(vir)}$. One

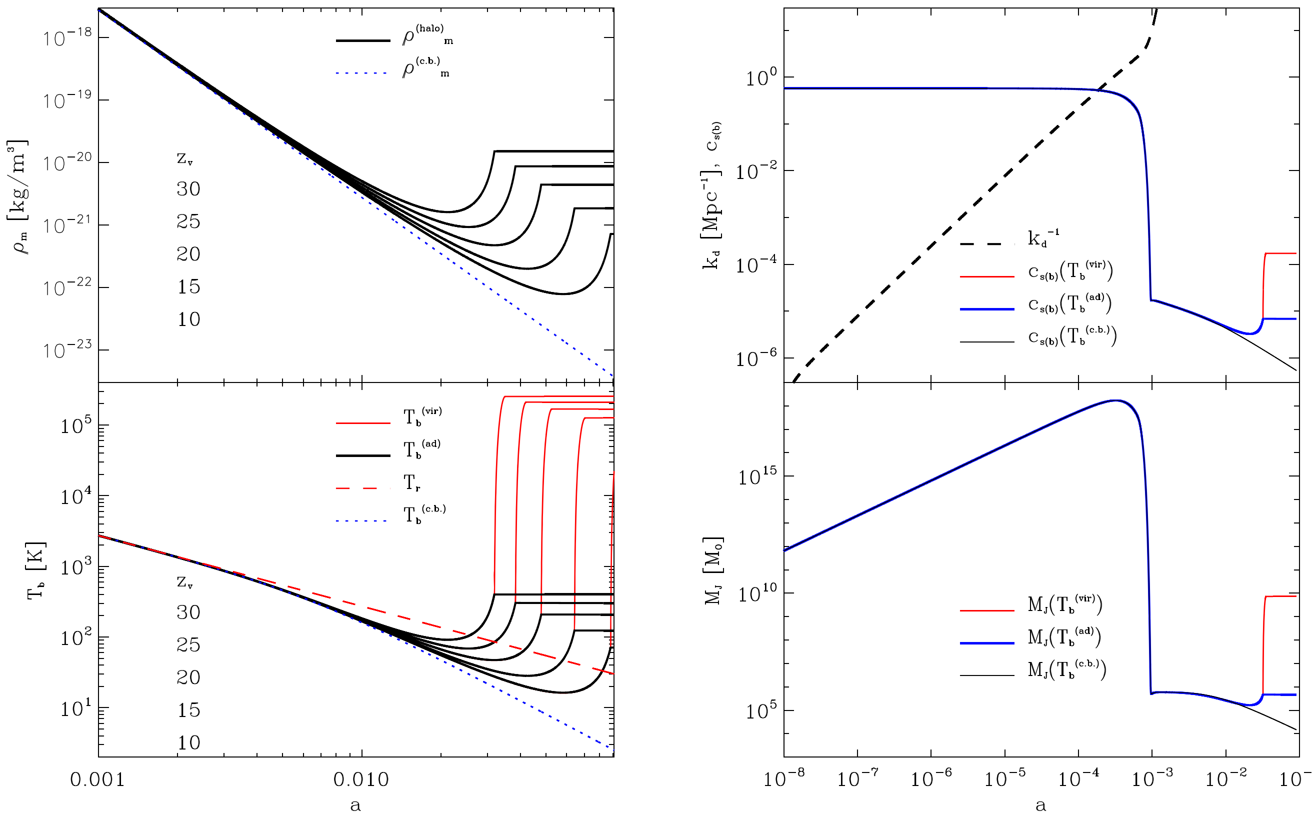

Figure 2. Left: evolution of density of matter $\rho_{\rm m}$ (top panel) and the temperature of baryonic matter $T_{\rm b}$ (bottom panel) for halos with $M_{\rm halo} = 7 \times 10^8\, M_\odot$ virialized at different redshifts $z_{\rm v}$. The corresponding values on the cosmological background (c.b.) are shown by dotted blue lines. The temperature of thermal relic radiation is shown by the dashed red lines. The adiabatic temperature of gas is shown by solid dark lines, and the virial temperature of gas is shown by red lines. Right: silk damping and effective sound speed in the baryonic matter before, during, and after cosmological recombination (top panel) and the Jeans scale for baryonic matter without molecular cooling (bottom panel). The thin solid dark lines show the same for the cosmological background.

can see that density and temperature of the gas are higher in halos that are formed earlier. This is in agreement with N-body simulations of large-scale structure formation (Klypin et al. 2011).

In the top panel of Figure 2 (right column) we show how the Silk damping scale $k_{\rm D}$ and the effective sound speed in the baryonic matter (in units of the speed of light c) vary with time through epochs. The transition of effective sound speed in the baryonic matter from the complete ionized ultrarelativistic stage to a practically neutral one in the dark ages we described phenomenologically as follows:

$$c_{\rm s(b)}^2 = \frac{1}{3(1+R)}\left(\frac{n_{\rm H\,II}}{n_{\rm H}}\right)^2 + \frac{\tilde{\gamma} k T_{\rm b}}{\mu_{\rm H} m_{\rm H} c}\left(\frac{n_{\rm H\,I}}{n_{\rm H}}\right)^2,$$

where the ionized and neutral fractions of hydrogen are accurately computed (see the next section).

Now we can estimate the variation of Jeans mass of baryonic matter through epochs on the c.b. and in the halo. Since the Jeans scale $\lambda_{\rm J} = (\pi c_{\rm s(b)}^2 / G\rho_{\rm b})^{1/2}$, the mass of baryonic matter in the sphere with radius $\lambda_{\rm J}/2$ is as follows:

$$M_{\rm J} = 7.2 \times 10^{10} \frac{c_{\rm s(b)}^3}{\sqrt{\rho_{\rm b}}}\, M_\odot,$$

where effective sound speed is in units of the speed of light and baryonic density is in units of kg m^{-3}. For $z < 800$ this formula gives practically the same values as Equation (40) from Galli & Palla (2013). The variation of Jeans mass through epochs is shown in bottom right panel of Figure 2. One can see that the baryonic matter cannot fragment into clumps of stellar mass without additional cooling; the Jeans mass is $>10^4\, M_\odot$.

Figure 1 has shown that the dark energy of a type of classical scalar field is slightly perturbed and practically does not influence the formation of dark matter halos. But the dark energy of other types can be disturbed essentially and can affect the virialization and final parameters of halos (Mota & van de Bruck 2004; Maor & Lahav 2005; Manera & Mota 2006; Nunes & Mota 2006; Creminelli et al. 2010; Wang & Fan 2012; Novosyadlyj et al. 2014). Let us show that for the type of dark energy with a low value of effective sound speed[5] the result can be different. In Novosyadlyj et al. (2014) it was shown that the static solution for some types of dark energy exists in the gravitational field of a spherical static halo. Since the ratio of "gravitational radius to radius of halo" is very small for the cases we are interested here, Equation (17) from Novosyadlyj et al. (2014) for the dark energy density at the center of the halo has a simple asymptotic for $c_{\rm s(de)} \neq 0$:

$$\frac{\rho_{\rm de}^{\rm st}}{\tilde{\rho}_{\rm de}(z_{\rm v})} = 1 + 1.47 \times 10^{-4} \frac{1 + w_{\rm de}}{c_{\rm s(de)}^2} (1 + z_{\rm v}) \Omega_{\rm m} h^2 (k\ {\rm Mpc})^{-2}. \quad (14)$$

We show in Figure 3 the evolution of density $\tilde{\delta}_{\rm de}$ and velocity $\tilde{v}_{\rm de}$ perturbations (left) and density (right) of such types of dark

[5] Cosmological observations practically do not constrain it (see, e.g., Sergijenko & Novosyadlyj 2015).

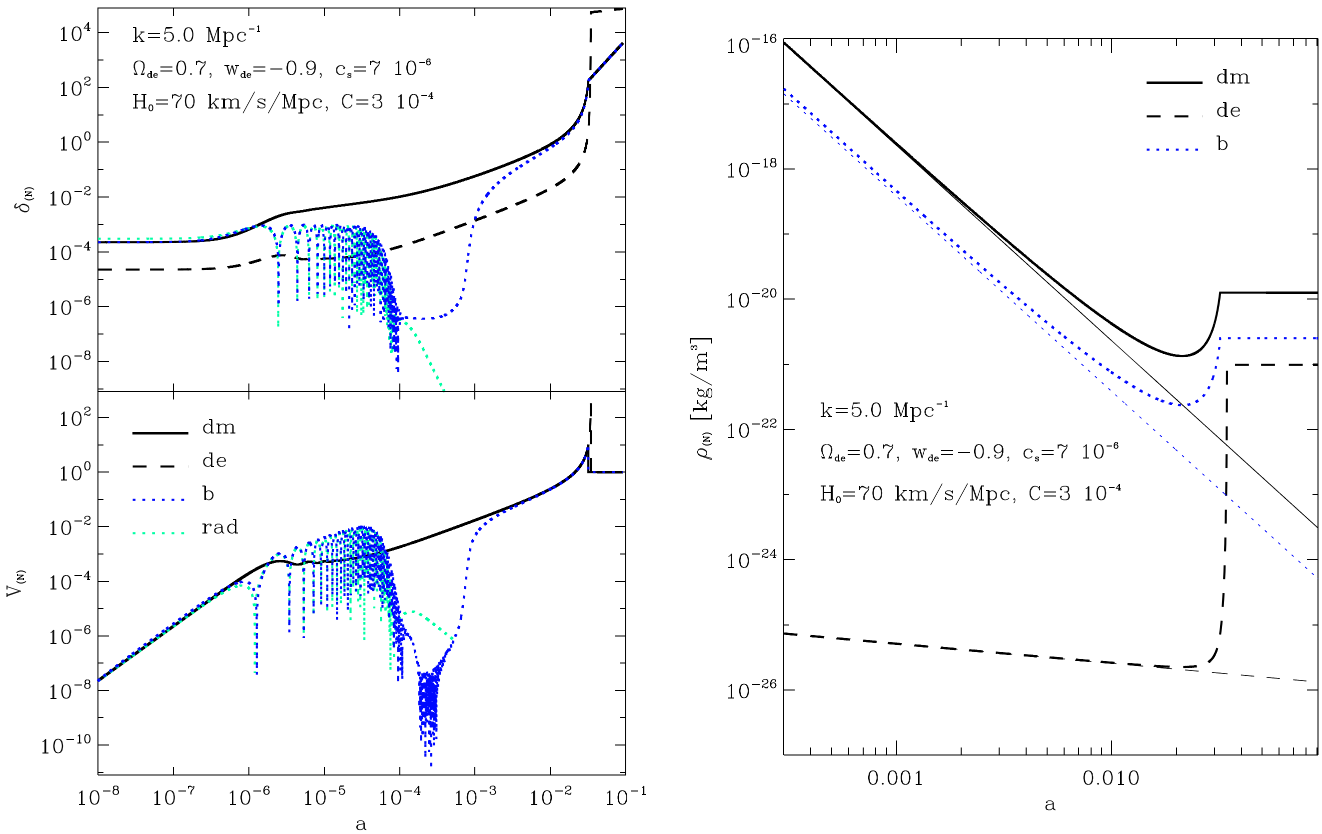

Figure 3. Left: evolution of density and velocity perturbations of matter, dark energy, baryons, and radiation that form a halo with virialized matter and dark energy, which reached the equilibrium state when the gravitational force is balanced by the pressure gradient. Right: density of dark matter (solid lines), dark energy (dashed lines), and baryonic gas (blue dotted lines). Thick lines: halo; thin lines: cosmological background.

energy with $c_{s(de)} \approx 7 \times 10^{-6}$ (which is close to $c_{s(b)}$ at the dark ages) in the model with the same cosmological and halo parameters as in the left panel of Figure 1. It is obtained in the following way: Equations (7) and (8) for dark energy are integrated up to the moment when the dark energy density reaches the static value (14), and then we put $\rho_{de} = \rho_{de}^{st}$ and $\tilde{v}_{de} = -\tilde{V}_H$. This means that after formation of a dark matter halo the dark energy continues to inflow until it reaches the equilibrium state where the gravitational force is balanced by the pressure gradient. This dark matter halo is formed at $z \approx 30.4$, and the density of dark energy reaches the static value (14) at $z \approx 28.1$, hence in ~12 Myr. One can see that for slightly lower values of $c_{s(de)}$ the density of dark energy in the halo will be comparable to main dark ages ingredients—dark matter and baryons.

3. Molecules in the Dark Age Halos

Let us estimate now the number densities of molecules in such halos and compare them with the corresponding values on the c.b. For that, we compute the fractions x_i of neutral atoms, molecules, and ions in the manner described in Galli & Palla (1998, 2013) and Novosyadlyj et al. (2017). The index "i" notes here and below any atom, molecule, or their ions presented in Table 1, where all chemical reactions are listed that are used here to estimate the chemistry composition of first halos. This is the minimal model, which consists of 19 reactions (Galli & Palla 1998): 10 for hydrogen, 6 for deuterium, and 3 for helium.

Table 1
Chemical Reactions (Their Notation in Brackets Corresponds to Galli & Palla 1998)

(H1)	$H^+ + e^- \rightarrow H + \gamma$	(H2)	$H + \gamma \rightarrow H^+ + e^-$
(H3)	$H + e^- \rightarrow H^- + \gamma$	(H4)	$H^- + \gamma \rightarrow H + e^-$
(H5)	$H^- + H \rightarrow H_2 + e^-$	(H7)	$H^- + H^+ \rightarrow H + H$
(H8)	$H + H^+ \rightarrow H_2^+ + \gamma$	(H9)	$H_2^+ + \gamma \rightarrow H + H^+$
(H10)	$H_2^+ + H \rightarrow H_2 + H^+$	(H15)	$H_2 + H^+ \rightarrow H_2^+ + H$
(D1)	$D^+ + e^- \rightarrow D + \gamma$	(D2)	$D + \gamma \rightarrow D^+ + e^-$
(D3)	$D + H^+ \rightarrow D^+ + H$	(D4)	$D^+ + H \rightarrow D + H^+$
(D8)	$D^+ + H_2 \rightarrow H^+ + HD$	(D10)	$HD + H^+ \rightarrow H_2 + D^+$
(He8)	$He + H^+ \rightarrow HeH^+ + \gamma$		
(He11)	$HeH^+ + H \rightarrow He + H_2^+$	(He14)	$HeH^+ + \gamma \rightarrow He + H^+$

The general form of the equation of chemical kinetics is as follows (Puy et al. 1993; Galli & Palla 1998; Vonlanthen et al. 2009):

$$aH\dot{x}_i = \sum_{mn} k_{mn}^{(i)} f_m f_n x_m x_n + \sum_m k_{m\gamma}^{(i)} f_m x_m - \sum_j k_{ij} f_i f_j x_i x_j - k_{i\gamma} f_i x_i, \quad (15)$$

where $k_{mn}^{(i)}$ are reaction rates for the reactants m and n, which lead to formation of atom/molecule/ion i, f_m is $f_{He} = n_{He}/n_H$ for reactant m containing helium, $f_D = n_D/n_H$ for reactant m containing deuterium, and $f_H \equiv 1$ for reactant m containing hydrogen only. For chemical species containing only hydrogen the fraction m is $x_{\rm m} = n_{\rm m}/n_{\rm H}$, where $n_{\rm m}$ is the number density of species m, and $n_{\rm H}$ is the total number density of hydrogen; for species containing deuterium and helium $x_{\rm m} = n_{\rm m}/n_{\rm D}$ and $x_{\rm m} = n_{\rm m}/n_{\rm He}$, respectively, where $n_{\rm D}$ and $n_{\rm He}$ are the total number densities of deuterium and helium. Equations (15) for reactions presented in Table 1, together with equations of cosmological recombinations for hydrogen, deuterium, and helium (Seager et al. 1999, 2000; Novosyadlyj et al. 2017), compose the system of equations of formation/recombination and dissociation/ionization of atoms and molecules, which are solved numerically for each step of integration of the system of Equations (6)–(12). We set the initial conditions for them at early epochs long before the cosmological recombination, when all ingredients were completely ionized and Saha approximation was applicable (see for details Appendix A in Novosyadlyj et al. 2017). The publicly available codes RecFast[6] and DDRIV1[7] have been used in the general code bdedmhalo.f, which was designed for integration of the system of Equations (6)–(12) with initial conditions (9) and (10) jointly with the system of Equations (15). In the computations we assumed $f_{\rm He} = 0.082$ and $f_{\rm D} = 2.61 \times 10^{-5}$, which follows from the standard model of cosmological nucleosynthesis and agrees with Planch2015 and other observational data. Reaction rates are taken from Galli & Palla (1998), except for the rates of recombination and photoionization of hydrogen and helium for $z > 200$, which are taken from Seager et al. (1999).

The results of join integration of these systems of equations are shown in Figure 4 for the halo with $M = 7 \times 10^8\,M_\odot$, initial amplitude $C = 3 \times 10^{-4}$, and two cases of halo temperature: in the virialized halo the gas has adiabatic temperature $T_{\rm b}^{\rm (ad)} = 400$ K (left panel) and virial temperature $T_{\rm b}^{\rm (vir)} = 253{,}800$ K (right panel). Before virialization in both cases, the temperature histories are the same. For comparison the same values for the c.b. are shown by thin blue lines. One can see that the differences in the concentrations of molecules in the halo and in the c.b. become noticeable in Figure 4 starting with $z = 100$ and reaching several orders for some molecules at $z = 10$. We present also results in the numbers in Table 2, with the number densities of atoms, ions, and molecules on the c.b. $n_{\rm i}^{\rm (c.b.)}$ and the ratio $n_{\rm i}^{\rm halo}/n_{\rm i}^{\rm (c.b.)}$ at different stages of halo formation: quasi-linear ($z = 100$), turnaround ($z_{\rm ta} \approx 46$), beginning of virialization ($z_{\rm v} \approx 30$), and the end of the dark ages ($z = 10$). They show that the number density of some molecules (H_2, HD) and molecular ions (H_2^+, H^-) in halos is higher than corresponding values on the c. b. caused by increased density and rates of reactions at quasi-linear and nonlinear evolution of density and velocity perturbations. At the same time, formation of some ingredients (H II, He II, HeH^+) is depressed: their number densities at the moment of virialization are lower than the density contrast $\Delta_{\rm v}$. For neutral atoms H I, D I, and He I the ratio of number densities $n_{\rm i}^{\rm halo}/n_{\rm i}^{\rm (c.b.)}$ increases by $((z_{\rm v} + 1)/11)^3 \approx 23$ times during the interval from $z_{\rm v}$ to $z = 10$, since fractions $x_{\rm i}$ are unchanged after virialization. For molecules, however, this ratio is different: for H_2 and HD, which are important coolers (Puy & Signore 1997), it is ∼140. For some molecules this ratio depends also on heating/cooling of baryonic gas in the virialization process. In our model when gas has a virial temperature, the number density of negative ions H^- is strongly depressed in the halo, while molecular ions HeH^+ practically disappear. These ions have the lowest binding energies (presented in parentheses near the notation of molecules in the table) for molecules studied here.

4. Discussions and Conclusions

We have analyzed the formation of spherical halos with $M \sim 10^8$–$10^9\,M_\odot$, which are virialized in the dark ages at $10 \leqslant z \leqslant 30$ in the four-component medium: dark matter, dark energy, baryons, and radiation. It is shown that dark matter halos can virialize at $z \approx 30$ if they are forming from high-density peaks in the Gaussian field of initial density perturbations with $\delta_{\rm m}^{\rm init} \sim 5$–$6\sigma_{\rm m}$, where $\sigma_{\rm m}$ are rms density fluctuations computed for the ΛCDM model with Planck2015 parameters. The dark matter halos that are forming from peaks with $\delta_{\rm m}^{\rm init} \sim 2$–$3\sigma_{\rm m}$ are virialized at $z \approx 10$; their number density (in units of $\rm Mpc^{-3}$) is close to the number density of bright galaxies estimated on the basis of galaxy redshift catalogs. The radiation component is important at the linear stage of evolution of precursors at the radiation-dominated epoch and at the decoupling time. The Silk damping effect depresses the amplitude of perturbations in the baryon–photon plasma before and during cosmological recombination (Figures 1–3).

The density and velocity perturbations in the dark energy component oscillate after entering the particle horizon when its effective sound speed is equal to the speed of light, as in the case when the classical scalar field is dark energy. In this case, the dark energy perturbations are not important for dynamics of halo formation after entering into the particle horizon (Figure 1). In the case when the effective sound speed is small, comparable to the effective sound speed in baryonic matter at the end of the dark ages, for example, then such dark energy can infall into forming halos of dark matter, reaching the state of hydrostatic equilibrium (Figure 3). Such dark energy can be important also at the late stage of halo formation.

The evolution of the baryonic component is most important since it can be observable. At the end of cosmological recombination the baryonic matter on the scales of interest here have been smoothed, but immediately after recombination it starts to free-fall into the potential wells of dark matter halo seeds; thus, the amplitudes of density and velocity perturbations in both components become practically the same at $z \approx 200$ (Figure 1). Further evolution of the dark matter and baryonic matter in the halo is the same up to the beginning of virialization, when the heating of gas makes its behavior again different. The gas in halos and on the c.b. had different dynamical and thermal histories, so the molecular fractions can be different too. To estimate such a difference, we have analyzed the kinetics of formation and dissociation of molecules and molecular ions in all stages of the dark matter halo formation: the linear and quasi-linear stages when dark matter overdensity expanded, and nonlinear stages when it turns around, collapses, and virializes. We have simplified the description of the last phase by stopping infall at the virial density $\rho_{\rm m}^{\rm (vir)} = \Delta_{\rm v}\rho_{\rm m}(a_{\rm v})$ (see details in Novosyadlyj et al. 2014). The temperature of gas was equal to the temperature of radiation up to $z \approx 800$; later it has been defined by adiabatic expansion before the turnaround and adiabatic compression after it, as is shown in the left panel of Figure 2 by dark solid

[6] http://www.astro.ubc.ca/people/scott/recfast.html
[7] http://www.netlib.org/slatec/src/ddriv1.f

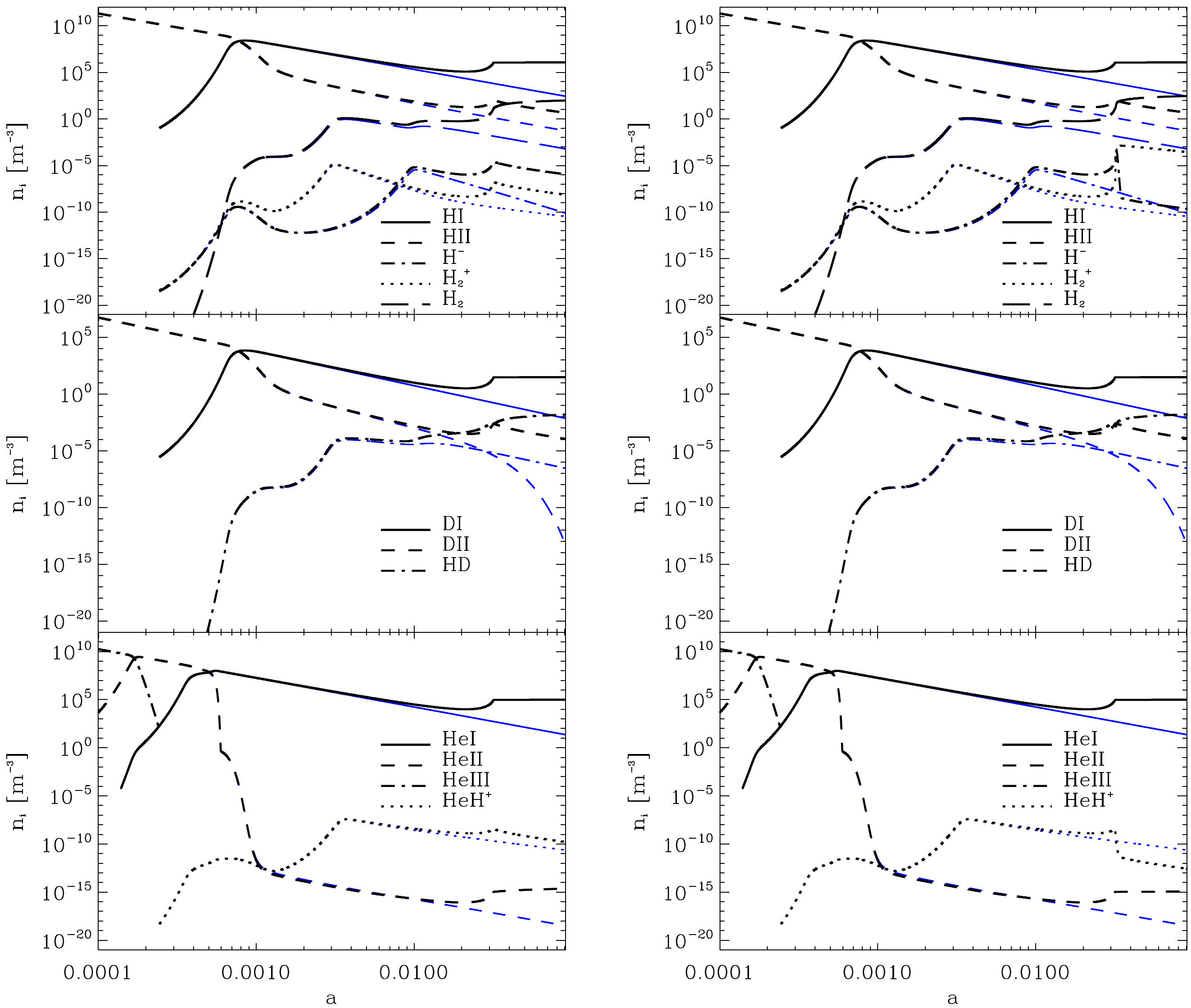

Figure 4. Evolution of the number density of atoms, ions, and neutral and ionized molecules during the dark ages on the cosmological background $n_i^{\rm (c.b.)}$ (blue lines) and in the central part of the spherical halo $n_{\rm i}^{\rm halo}$ with $M = 7 \times 10^8\,M_\odot$, which have been virialized at $z \sim 30$ (black lines). In the left panel the gas in the virialized halo has adiabatic temperature ($T_{\rm b}^{\rm (ad)} = 400$ K), and in the right panel the gas in the virialized halo has virial temperature ($T_{\rm b}^{\rm (vir)}$= 253,800 K).

Table 2

Number Densities of Atoms, Ions, and Molecules on the Cosmological Background $n_{\rm i}^{\rm (c.b.)}$ and Ratio $n_{\rm i}^{\rm halo}/n_{\rm i}^{\rm (c.b.)}$ at Different Stages of Halo Formation

Species (Binding Energy)	$z = 100$		$z = 46.06$		$z = 30.35$		$z = 10$		
	$n_{\rm i}^{\rm (c.b.)}$	$\frac{n_{\rm i}^{\rm halo}}{n_{\rm i}^{\rm (c.b.)}}$	$n_{\rm i}^{\rm (c.b.)}$	$\frac{n_{\rm i}^{\rm halo}}{n_{\rm i}^{\rm (c.b.)}}$	$n_{\rm i}^{\rm (c.b.)}$	$\frac{n_{\rm i}^{\rm halo}}{n_{\rm i}^{\rm (c.b.)}}$	$n_{\rm i}^{\rm (c.b.)}$	$\frac{n_{\rm i}^{\rm halo}}{n_{\rm i}^{\rm (c.b.)}}(T_{\rm b}^{\rm (ad)})$	$\frac{n_{\rm i}^{\rm halo}}{n_{\rm i}^{\rm (c.b.)}}(T_{\rm b}^{\rm (vir)})$
H I (13.60 eV)	2.1×10^5	1.8	2.2×10^4	5.6	6.3×10^3	178	2.8×10^2	4.1×10^3	4.1×10^3
H II	51.4	1.5	4.6	4.0	1.3	81	5.4×10^{-2}	86	87
H^- (0.754 eV)	3.1×10^{-6}	2.1	1.2×10^{-7}	8.7	1.6×10^{-8}	1570	8.0×10^{-11}	1.4×10^4	2.8
H_2 (4.47 eV)	0.13	2.9	4.6×10^{-2}	13.0	1.4×10^{-2}	1010	6.2×10^{-4}	1.5×10^5	4.7×10^5
H_2^+ (2.77 eV)	2.2×10^{-8}	1.8	9.5×10^{-10}	4.8	3.3×10^{-10}	510	3.5×10^{-11}	212	7.8×10^6
D I (15.47 eV)	5.6	1.8	0.56	5.6	0.17	178	7.2×10^{-3}	4.1×10^3	4.1×10^3
D II	1.0×10^{-3}	1.5	4.3×10^{-5}	7.0	3.7×10^{-6}	662	4.7×10^{-14}	2.3×10^9	2.6×10^9
HD (4.51 eV)	3.6×10^{-5}	2.4	2.0×10^{-5}	21.3	6.5×10^{-6}	386	2.8×10^{-7}	5.3×10^4	5.6×10^4
He I (24.59 eV)	1.8×10^4	1.8	1.8×10^3	5.6	5.3×10^2	178	22.7	4.1×10^3	4.1×10^3
He II (54.44 eV)	1.8×10^{-16}	1.2	2.1×10^{-17}	4.0	6.8×10^{-18}	159	3.3×10^{-19}	7.0×10^3	3.3×10^3
HeH^+ (1.85 eV)	2.8×10^{-9}	1.4	4.9×10^{-10}	2.7	2.0×10^{-10}	18	2.3×10^{-11}	7	1.2×10^{-2}

lines for halos virialized at $10 \leqslant z \leqslant 30$. Thin solid red lines show the virial temperatures (13) of these halos, which we set by smoothly transitioning from the adiabatic value to the virial one for a short time corresponding to $\Delta a = 0.1 a_v$ immediately after a_v. One can see that in any case the key parameters of virialized halos—density and temperature—are defined by the moment of virialization a_v.

The estimated number densities of atoms, molecules, and their ions in halos are essentially larger than on the c.b. At the moment of halo turnaround the number densities of neutral atoms H I, D I, and He I are 5.6 times larger than corresponding values on the c.b. Such a ratio of number densities equals the density contrast for a top-hat halo, which follows from the well-known Tolman model of a dust-like spherical cloud. For the number density of molecules H_2 and HD, which are important coolers of dark ages protostar clouds, these ratios are 13 and 21, respectively (Table 2, third column). For the moment when the density contrast of a collapsing halo reaches the contrast $\Delta_v \approx 178$, following from the virial theorem, the ratios $n_i^{\rm halo}/n_i^{\rm (c.b.)}$ for H_2 and HD are $\approx$1000 and $\approx$400, respectively, while for the neutral atoms H I, D I, and He I they are equal to 178. This effect is explained by the crucial dependence of chemical reaction chains, which lead to formation of these molecules, on the local density and temperature of hydrogen–deuterium slightly ionized gas. Taking into account this effect for computation of cooling/heating processes in the dark ages halos can help us resolve the problem of fragmentation of the primordial medium into protostar clouds with mass $\lesssim 10^3\,M_\odot$. We plan to do that in the next work.

This work was supported by the International Center of Future Science of Jilin University (P.R. China) and the project of Ministry of Education and Science of Ukraine “Dynamics, evolution and physical effects in the formation of structure of the universe, supernova remnants and close binary stars with relativistic components” (state registration no. 0116U001544).

ORCID iDs

V. Shulga https://orcid.org/0000-0001-6529-5610

References

Aver, E., Olive, K. A., Porter, R., & Skillman, E. D. 2013, JCAP, 1311, 017
Barkana, R., & Loeb, A. 2001, PhR, 349, 125
Bromm, V., & Yoshida, N. 2011, ARA&A, 49, 373
Creminelli, P., D’Amico, G., Norena, J., Senatore, L., & Vernizzi, F. 2010, JCAP, 03, 027
Dalgarno, A., & Lepp, S. 1987, in Proc. IAU Symp., Astrochemistry, ed. S. P. Tarafdar & M. P. Varshni (Dordrecht: Reidel), 109
Demianski, M., & Doroshkevich, A. G. 2014, MNRAS, 439, 179
Dubrovich, V. K. 1977, SvAL, 3, 128
Fixsen, D. J. 2009, ApJ, 707, 916
Galli, D., & Palla, F. 1998, A&A, 335, 403
Galli, D., & Palla, F. 2013, ARA&A, 51, 163
Gay, C. D., Stancil, P. C., Lepp, S., & Dalgarno, A. 2011, ApJ, 737, 44
Hirata, C. M., & Padmanabhan, N. 2006, MNRAS, 372, 1175
Hu, W., & Sugiyama, N. 1995, ApJ, 444, 489
Hu, W., & Sugiyama, N. 1996, ApJ, 471, 542
Izotov, Y. I., & Kolesnik, I. G. 1984, SvA, 28, 15
Klypin, A., Trujillo-Gomez, S., & Primack, J. 2011, ApJ, 740, 102
Kulinich, Yu., & Novosyadlyj, B. 2003, JPhSt, 7, 234
Lepp, S., & Shull, M. 1984, ApJ, 280, 465
Lepp, S., & Stancil, P. C. 1998, in The Molecular Astrophysics of Stars and Galaxies, ed. T. W. Hartquist & D. A. Williams (Oxford: Clarendon), 37
Lepp, S., Stancil, P. C., & Dalgarno, A. 2002, JPhB, 35, 57
Lewis, A., Challinor, A., & Lasenby, A. 2000, ApJ, 538, 473
Manera, M., & Mota, D. F. 2006, MNRAS, 371, 1373
Maor, I., & Lahav, O. 2005, JCAP, 07, 003
Mota, D., & van de Bruck, C. 2004, A&A, 421, 71
Novosyadlyj, B., Kulinich, Yu., & Tsizh, M. 2014, PhRvD, 90, 063004
Novosyadlyj, B., Sergijenko, O., & Shulga, V. M. 2017, KPCB, 33, 255
Novosyadlyj, B., Tsizh, M., & Kulinich, Y. 2016, GReGr, 48, 30
Nunes, N. J., & Mota, D. F. 2006, MNRAS, 368, 751
Oh, S. P., & Haiman, Z. 2002, ApJ, 569, 558
Padmanabhan, T. 2002, Theoretical Astrophysics, Volume III: Galaxies and Cosmology (Cambridge: Cambridge Univ. Press), 619
Planck Collaboration, Ade, P. A. R., Aghanim, N., et al. 2016, A&A, 594, A13
Puy, D., Alecian, G., Le Bourlot, J., et al. 1993, A&A, 267, 337
Puy, D., & Signore, M. 1997, NewA, 2, 299
Puy, D., & Signore, M. 2002, NewAR, 46, 709
Safranek-Shrader, C., Bromm, V., & Milosavljevic, M. 2010, ApJ, 723, 1568
Scott, D., & Moss, A. 2009, MNRAS, 397, 445
Seager, S., Sasselov, D. D., & Scott, D. 1999, ApJL, 523, L1
Seager, S., Sasselov, D. D., & Scott, D. 2000, ApJS, 128, 407
Sergijenko, O., & Novosyadlyj, B. 2015, PhRvD, 91, 083007
Stancil, P., Lepp, S., & Dalgarno, A. 1998, ApJ, 509, 1
Vonlanthen, P., Rauscher, T., Winteler, C., et al. 2009, A&A, 503, 47
Wang, Q., & Fan, Z. 2012, PhRvD, 85, 023002